Human Head Exposure to Bluetooth Frequency - Thermal Response

H. Dodig, Faculty of Maritime Studies, University of Split, Croatia
K. Viđak, FESB, University of Split, Croatia
M. Škiljo, FESB, University of Split, Croatia
D. Poljak, FESB, University of Split, Croatia

This work was supported by the Croatian Science Foundation under the project number HRZZ- IPS-2024-02-7779

Paper Outline

- **Goal**: numerical computation of steady state thermal response in human head due to bluetooth frequencies

- **Steps involved:**
- Human head model (geometry and tissues)
- Numerical computation of electromagnetic fields – inhomogenous EM scattering problem – compute SAR
- Numerical computation of thermal response caused by electromagnetic fields – solving Pennes bio-heat equation

Introduction

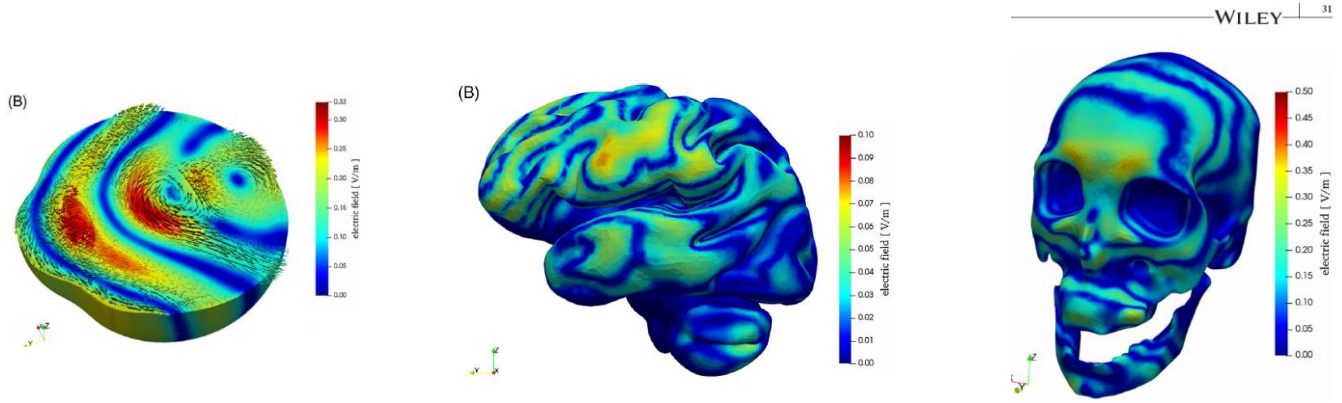

- Established biological effect of EM fields in the bluetooth frequency range (2.402 GHz – 2.480 GHz) is tissue heating
- Related specific absorption rate (SAR) quantifies how much EM energy is absorbed per unit mass of tissue
- Human head is of particular interest as it contains critical organs (eyes, brain, eairs)
- Numerical methods indespensable – direct methods of measurement are very difficult
- Goal is to compare numerical results to real world measurements on IEEE recommended phantom (IEEE SAM model)

Human head model

- The geometrical (CAD) model is obtained from MRI images
- In previous work we were involved with inhomogeneous head models
- Because one of the aims of this work is to compare numerical methods to real world measurements (as a part of HRZZ project) numerical methods were applied to homogeneous head model

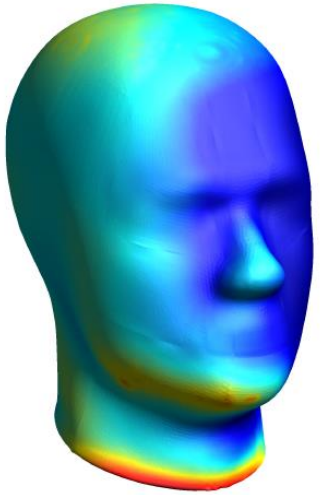

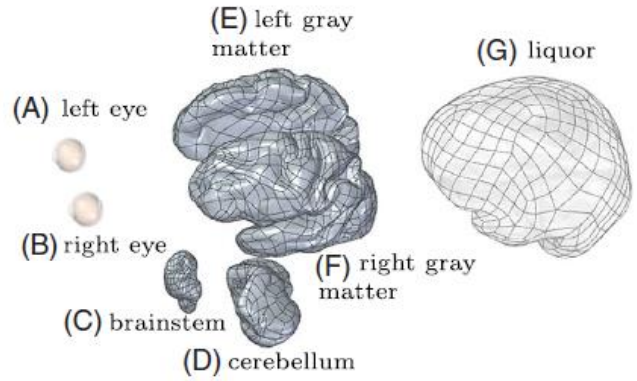

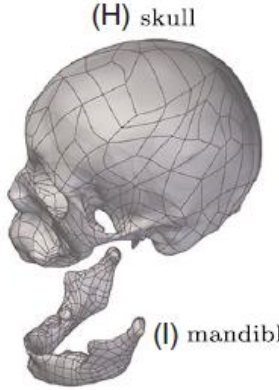

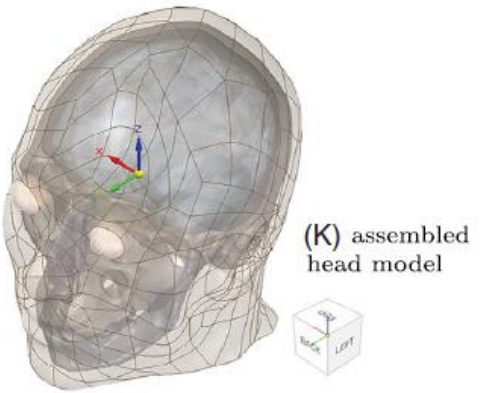

EM fields computation

- Human head – treated as a time harmonic EM scattering problem
- Time harmonic EM wave is impinging on the computational boundary Γ
- The choice of methods is various, each has advantages and disadvantages:
  - FDTD
  - FEM+PML
  - MoM/FEM
  - BEM/FEM

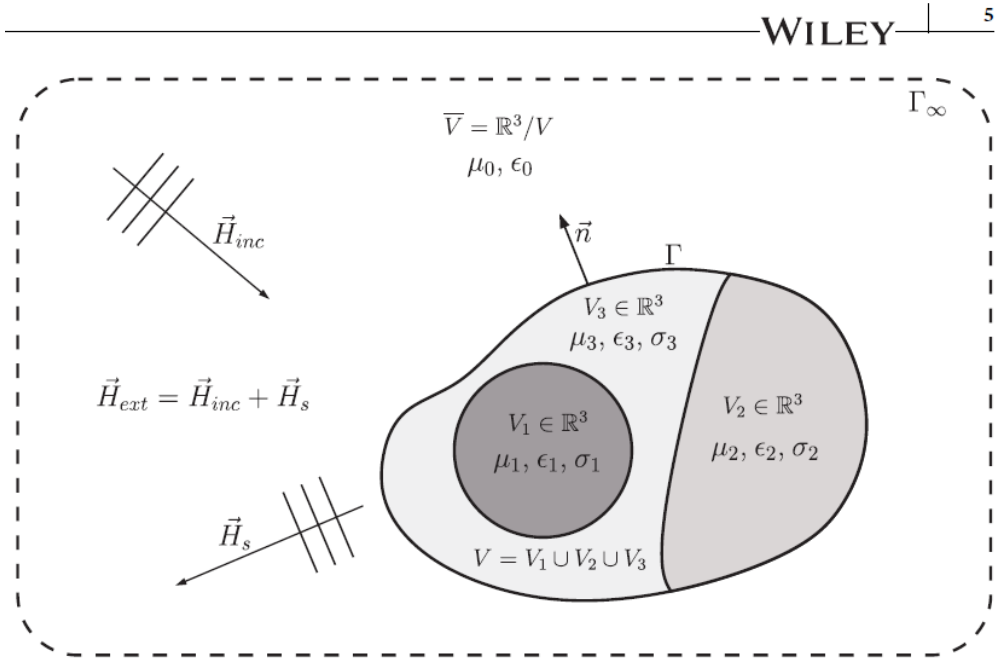

EM fields computation

- Hybrid MoM/FEM & BEM/FEM methods are computationally expensive
- Computational costs are mostly due to MoM or BEM as these methods produce dense matrices
- These computational costs are due to number of unknowns (related to number of triangles) at the bounding surface of the model

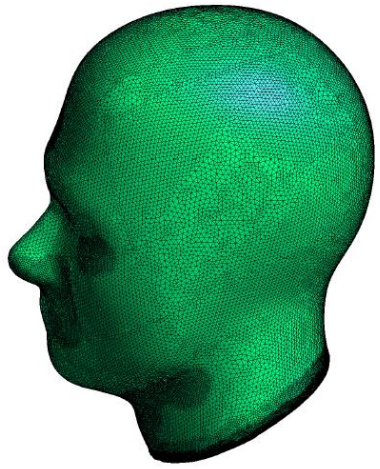

Fig. 3. The surface of the phantom head is represented by 151,185 triangles, and the interior of the head is represented by 3,511,924 tetrahedrons.

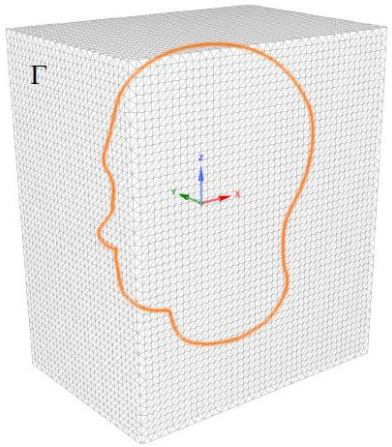

Fig. 4. The surface of the airbox is discretized using only 8,984 triangles yielding 13,476 unique edges, and $2 \times 13,476$ unknown coefficients e_b and h_b at the surface Γ.

EM fields computation

- The method of choice is hybrid BEM/FEM with Nedelec edge elements, which enforce tangential continuity of the EM fields
- The bounding surface Γ is modeled with triangular edge elements and the interior is modeled with tetrahedral edge elements
- Unknowns are related to the edges of elements

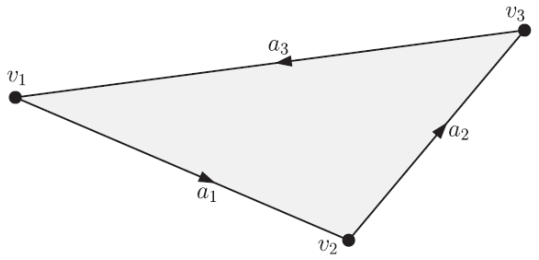

Edge # (i)	First endpoint (p)	Second endpoint (q)
1	1	2
2	2	3
3	3	1

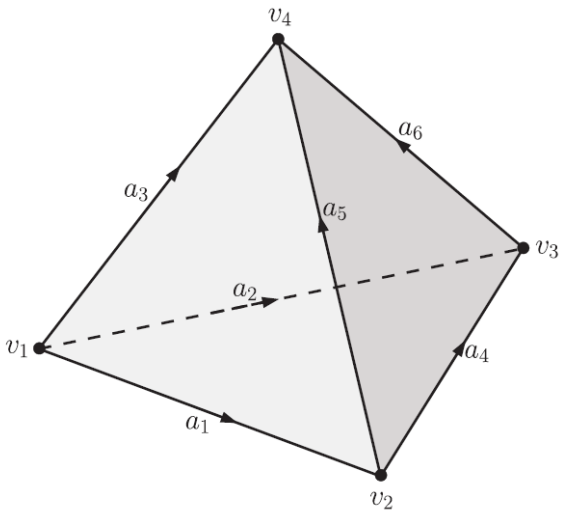

Edge # (i)	First endpoint (p)	Second endpoint (q)
1	1	2
2	1	3
3	1	4
4	2	3
5	2	4
6	3	4

EM fields computation

- The formulation begins with time-harmonic version of Maxwell equations for EM fields

$$\nabla \cdot \vec{D}_{ext} = \rho,$$

$$\nabla \cdot \vec{B}_{ext} = 0,$$

$$\nabla \times \vec{E}_{ext} = -\frac{\partial \vec{B}_{ext}}{\partial t},$$

$$\nabla \times \vec{H}_{ext} = \vec{J}_{ext} + \frac{\partial \vec{D}_{ext}}{\partial t},$$

- After some manupulation one arrives to the magnetic field integral equation:

$$\alpha(\vec{r})\vec{H}_{ext}(\vec{r}) = \vec{H}_{inc}(\vec{r}) + \oint_{\Gamma} \nabla' G(\vec{r},\vec{r}') \left(\vec{H}_{ext}(\vec{r}') \cdot d\vec{S}'\right) + \oint_{\Gamma} d\vec{S}' \times \left(G(\vec{r},\vec{r}')\nabla' \times \vec{H}_{ext}(\vec{r}')\right) + \oint_{\Gamma} \left(d\vec{S}' \times \vec{H}_{ext}(\vec{r}')\right) \times \nabla' G(\vec{r},\vec{r}'),$$

H. Dodig, D. Poljak, M. Cvetković, „On the edge element boundary element method/finite element method coupling for time harmonic electromagnetic scattering problems”, Int J Numer Methods Eng. 2021;1–40, DOI: 10.1002/nme.6675

EM fields computation

- Fields external to Γ, and the fields internal Γ to are coupled using standard EM jump conditions for EM fields:

$$\vec{n} \times \vec{H}_{ext} = \vec{n} \times \vec{H},$$

$$\vec{n} \times \vec{E}_{ext} = \vec{n} \times \vec{E}.$$

- after some manipulation one arrives to the following BIE:

$$\alpha \vec{H} \times \vec{n} = \vec{H}_{inc} \times \vec{n} + \vec{n} \times \frac{j}{\omega_0 \mu_0} \oint_\Gamma \nabla' G \left(\nabla'_s \cdot \vec{n}' \times \vec{E}' \right) dS'$$
$$- j\omega\epsilon_0 \vec{n} \times \oint_\Gamma d\vec{S}' \times G\vec{E}'$$
$$- \vec{n} \times \oint_\Gamma \left(d\vec{S}' \times \vec{H}' \right) \times \nabla' G.$$

H. Dodig, D. Poljak, M. Cvetković, „On the edge element boundary element method/finite element method coupling
for time harmonic electromagnetic scattering problems”, Int J Numer Methods Eng. 2021;1–40, DOI: 10.1002/nme.6675

EM fields computation

- Previous boundary integral equation is not enough to establish solvable system of equations
- To form system of equations we take dot product of previous BIE with vectorial basis functions $\delta_i \overrightarrow{W_i}$ - (FEM of BEM)

Surface integral of surface integral

$$\oint_\Gamma d\vec{S} \cdot \delta_i \vec{W}_i^{\Delta} \times \vec{H} = \oint_\Gamma d\vec{S} \cdot \frac{1}{\alpha} \delta_i \vec{W}_i^{\Delta} \times \vec{H}_{inc} - \frac{j}{\omega_0 \mu_0} \oint_\Gamma d\vec{S} \cdot \frac{1}{\alpha} \delta_i \vec{W}_i^{\Delta} \times \oint_\Gamma \nabla' G \left(\nabla_s' \cdot \vec{n}' \times \vec{E}' \right) dS'$$
$$+ j\omega\epsilon_0 \oint_\Gamma d\vec{S} \cdot \frac{1}{\alpha} \delta_i \vec{W}_i^{\Delta} \times \oint_\Gamma d\vec{S}' \times G\vec{E}'$$
$$+ \oint_\Gamma \frac{1}{\alpha} d\vec{S} \cdot \delta_i \vec{W}_i^{\Delta} \times \oint_\Gamma \left(d\vec{S}' \times \vec{H}' \right) \times \nabla' G.$$

H. Dodig, D. Poljak, M. Cvetković, „On the edge element boundary element method/finite element method coupling
for time harmonic electromagnetic scattering problems", Int J Numer Methods Eng. 2021;1–40, DOI: 10.1002/nme.6675

EM fields computation

- The integration procedure involves computation of double surface integrals:

$$\begin{bmatrix} G_{11}^1+G_{11}^2 & G_{12}^1+G_{12}^2 & G_{13}^1+G_{13}^2 \\ G_{21}^1+G_{21}^2 & G_{22}^1+G_{22}^2 & G_{23}^1+G_{23}^2 \\ G_{31}^1+G_{31}^2 & G_{32}^1+G_{32}^2 & G_{33}^1+G_{33}^2 \end{bmatrix} \begin{Bmatrix} e_{j_1} \\ e_{j_2} \\ e_{j_3} \end{Bmatrix} + \begin{bmatrix} H_{11}^2+H_1^1 & H_{12}^2 & H_{13}^2 \\ H_{21}^2 & H_{22}^2+H_2^1 & H_{23}^2 \\ H_{31}^2 & H_{32}^2 & H_{33}^2+H_3^1 \end{bmatrix} \begin{Bmatrix} h_{j_1} \\ h_{j_2} \\ h_{j_3} \end{Bmatrix} = \begin{Bmatrix} H_1^{inc} \\ H_2^{inc} \\ H_3^{inc} \end{Bmatrix}$$

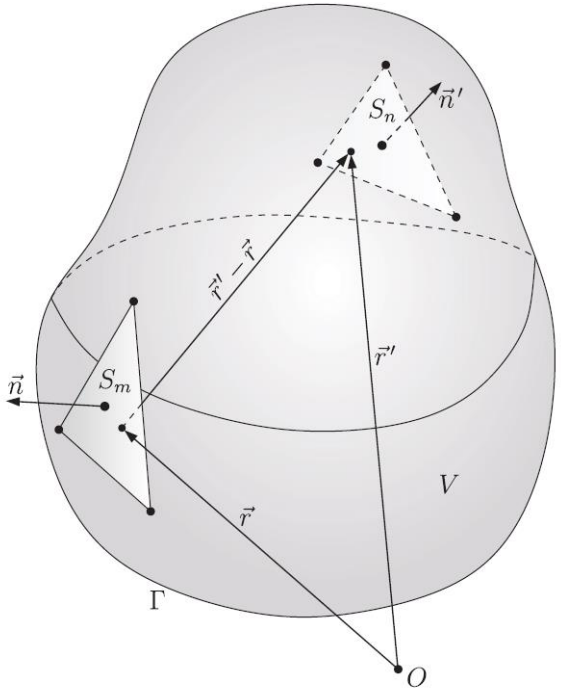

$$G_{ij}^1 = \frac{j}{\omega_0\mu_0}\int_{S_m} d\vec{S}\cdot\frac{1}{\alpha}\delta_{im}\vec{W}_{in}^{\Delta}\times\int_{S_n}\nabla' G\left(\nabla_s'\cdot\vec{n}'\times\delta_{jm}\vec{W}_{jm}^{\Delta}\right)dS',$$

$$G_{ij}^2 = -j\omega\epsilon_0\int_{S_m} d\vec{S}\cdot\frac{1}{\alpha}\delta_{in}\vec{W}_{in}^{\Delta}\times\int_{S_n} d\vec{S}'\times G\delta_{jm}\vec{W}_{jm}^{\Delta},$$

$$H_i^1 = \int_{S_m} d\vec{S}\cdot\delta_{in}\vec{W}_{in}^{\Delta}\times\delta_{im}\vec{W}_{im}^{\Delta},$$

EM fields computation

- FEM part relies on Galerkin method of weighted residuals:

$$\int_V \delta_i \vec{W}_i \cdot \left[\nabla \times \left(\frac{j}{\omega \mu} \nabla \times \vec{E} \right) - (\sigma + j\omega\epsilon) \vec{E} \right] dV = 0,$$

- where the vectorial basis functions $\overrightarrow{W_i}$ are based on nodal basis functions:

$$\vec{W}_i = N_p \nabla N_q - N_q \nabla N_p,$$

- and the field expansion is approximated as:

$$\vec{E} = \sum_{j=1}^{3} \delta_j \vec{W}_j e_j,$$

$$\vec{H} = \sum_{j=1}^{3} \delta_j \vec{W}_j^{\Delta} h_j,$$

Why tangential edge elements?

- Double surface integrals can be converted to contour integrals
- Reduces computational time and improves accuracy
- Easier to deal with singularities in BEM

$$\alpha(\vec{r})\phi(\vec{r}) = \oint_{\partial V} dS' \left[G(\vec{r},\vec{r}\,') \frac{\partial \phi(\vec{r}\,')}{\partial \vec{n}\,'} - \phi(\vec{r}\,') \frac{\partial G(\vec{r},\vec{r}\,')}{\partial \vec{n}\,'} \right]$$

$$I_1(\vec{r}) = \int_{S_\Delta} N_i(\vec{r}\,') G(R) dS', \qquad I_1(\vec{r}) = \sum_{i-1}^{3} \int_{e_i} u(R) \left[\vec{a}_i + b_i(\vec{r}) \vec{q} \right] \cdot d\vec{l} = \sum_{i-1}^{3} I_1^i(\vec{r}),$$

$$I_2(\vec{r}) = \int_{S_\Delta} N_i(\vec{r}\,') \frac{\partial G(R)}{\partial \vec{n}\,'} dS', \qquad I_2(\vec{r}) = -\vec{n}\,' \cdot \nabla \oint_{\partial S_\Delta} u(R) \left[\vec{a}_i + b_i(\vec{r}) \vec{q} \right] \cdot d\vec{l}\,'$$

H. Dodig, M. Cvetković, D. Poljak „ ON THE COMPUTATION OF SINGULAR INTEGRALS OVER TRIANGULAR SURFACES IN R3”, Boundary Elements and other Mesh Reduction Methods XLI, 2019;1–40, doi:10.2495/BE410091

EM fields computation

- Finally, BEM and FEM are combined into a system of equations:

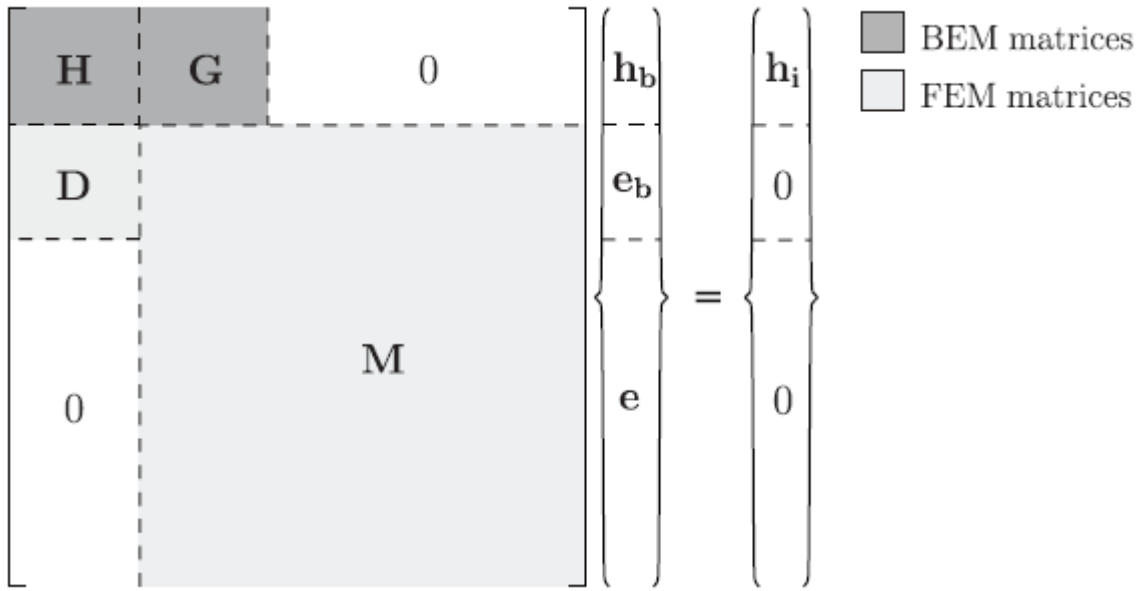

- Although submatrices related to BEM bear less unknowns, the computational cost of solving the matrix and filling the matrix surpasses the FEM part by far

EM fields computation

- This EM computational method was tested and improved over the course of decades (since 2008)

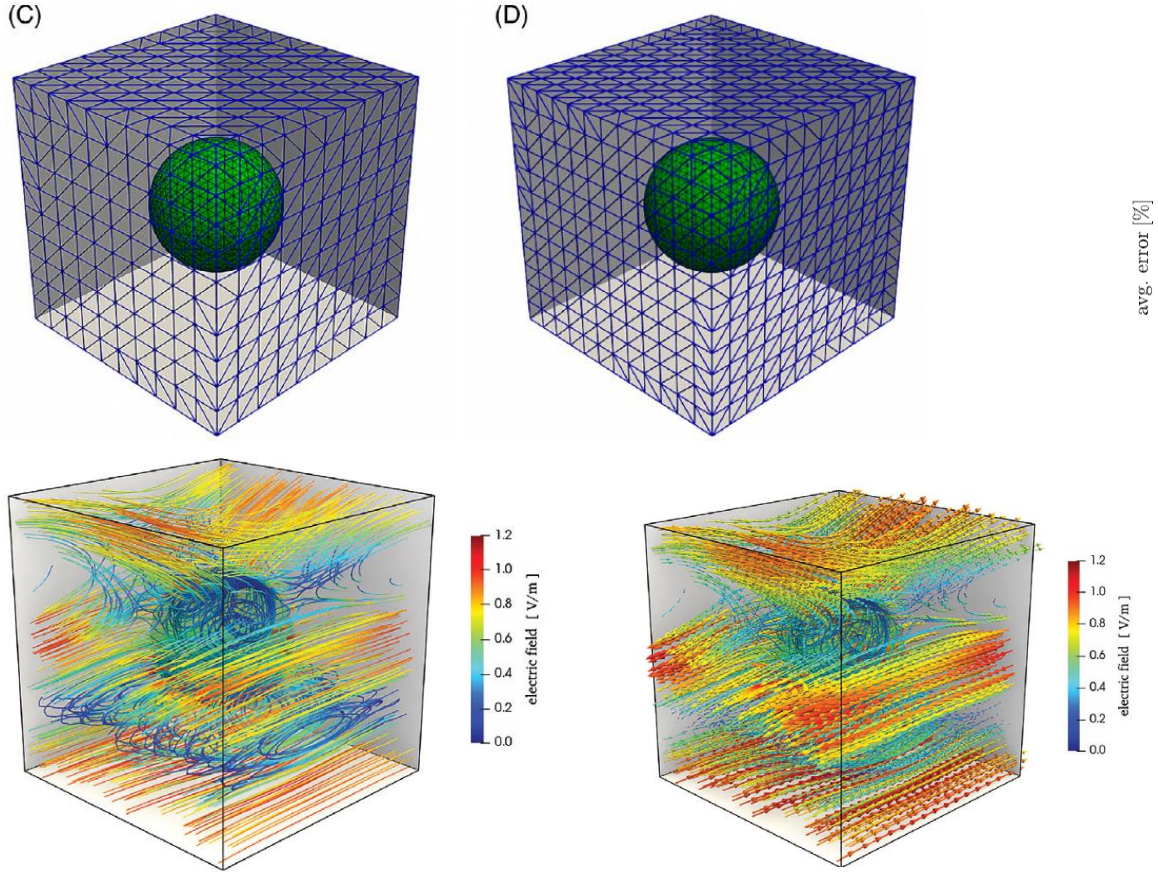

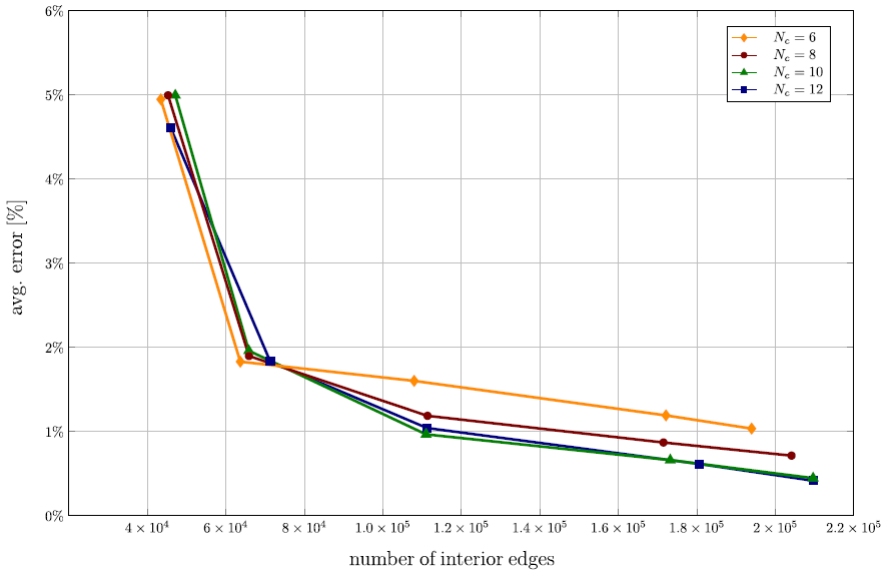

EM fields computation

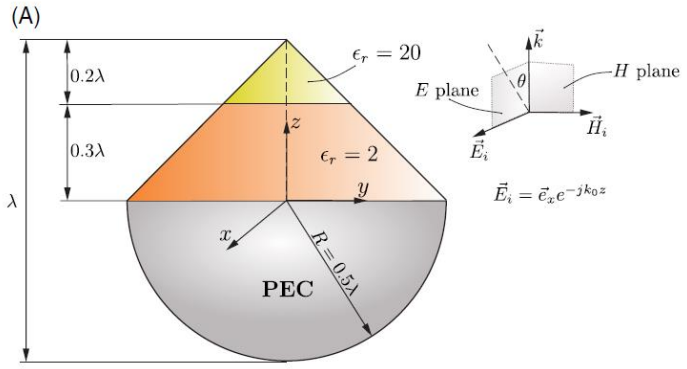

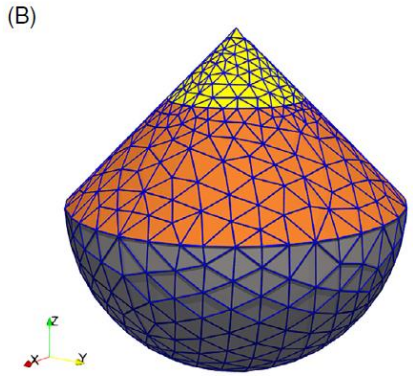

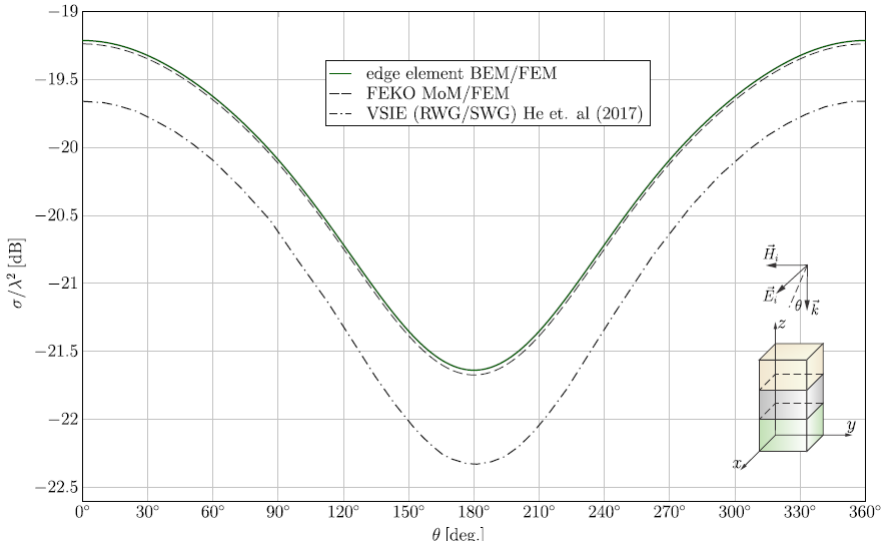

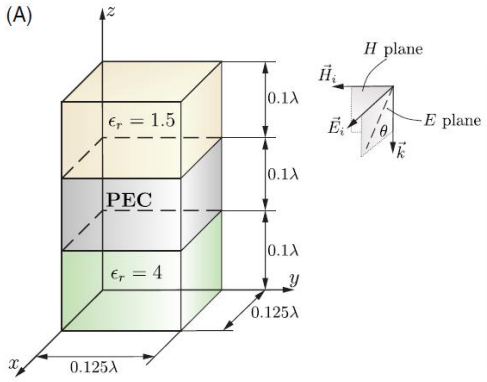

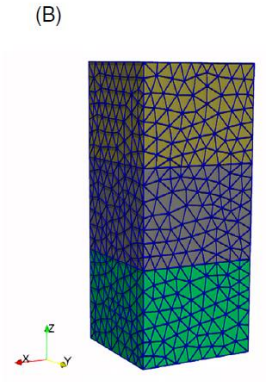

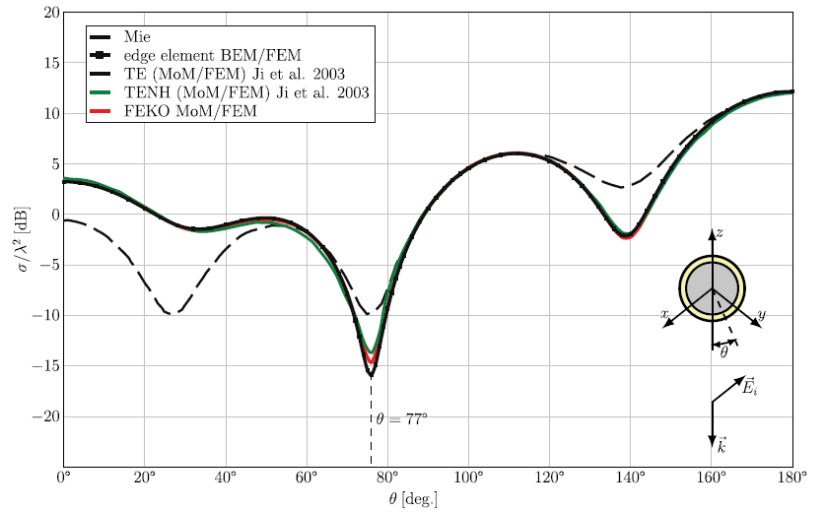

EM fields computation

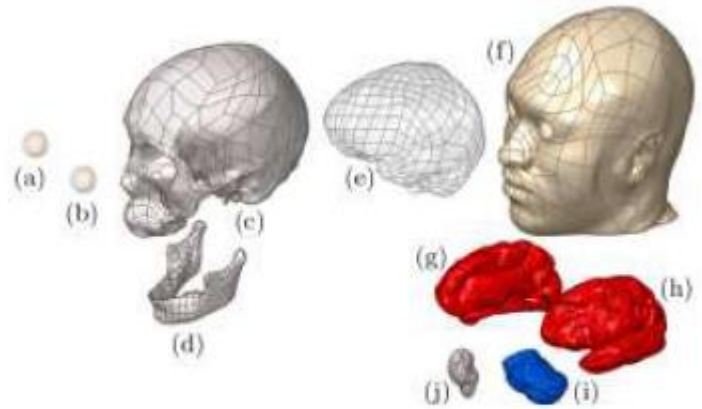

Fig. 2. Exploded view of CAD model used for electromagnetic and thermal simulation. Main tissues used for simulations are (a) left eye, (b) right eye, (c) skull, (d) mandible, (e) CSF, (f) skin, (g) left gray matter, (h) right gray matter, (i) cerebellum, and (j) brain stem. Geometry of all tissues except eyes is obtained from MRI scans [23].

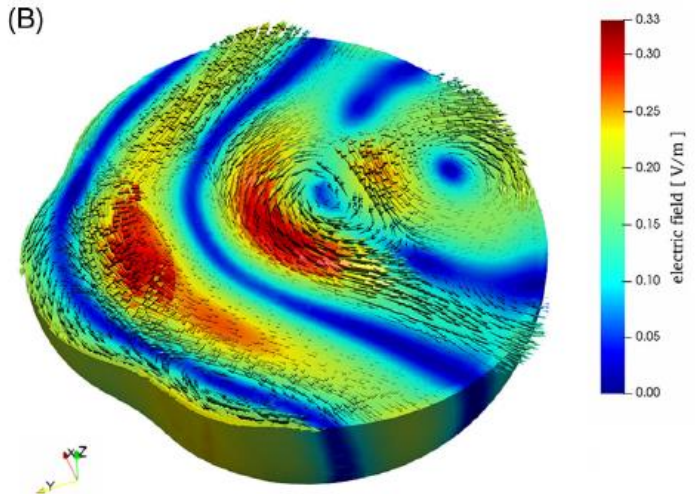

Cross section of left eye in $x - y$ plane with removed corneal surface.

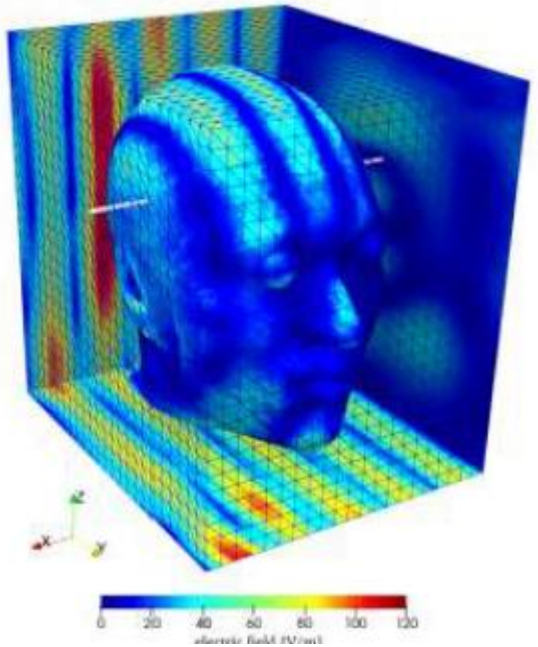

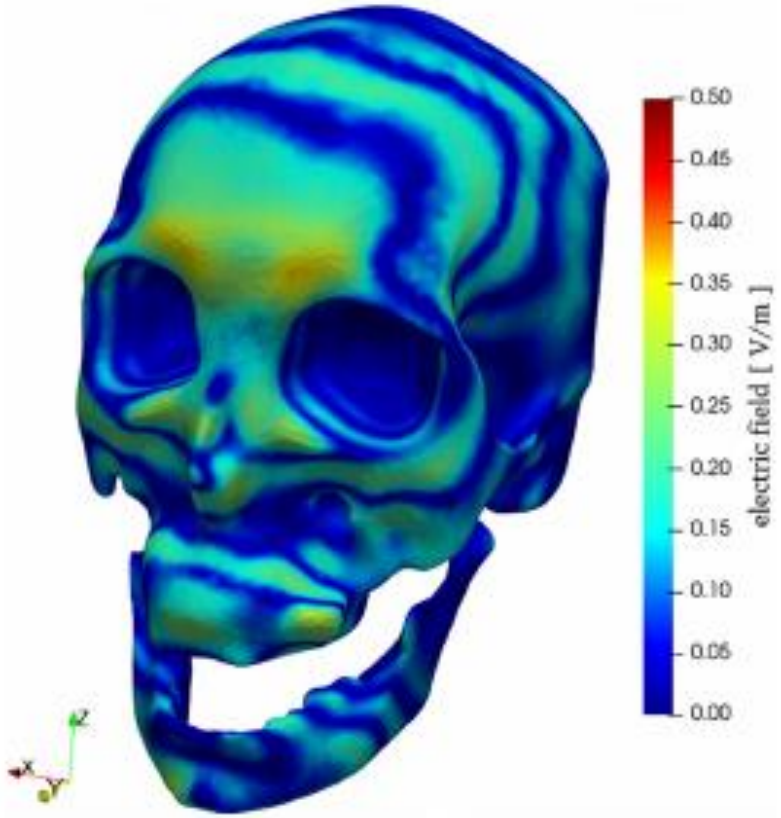

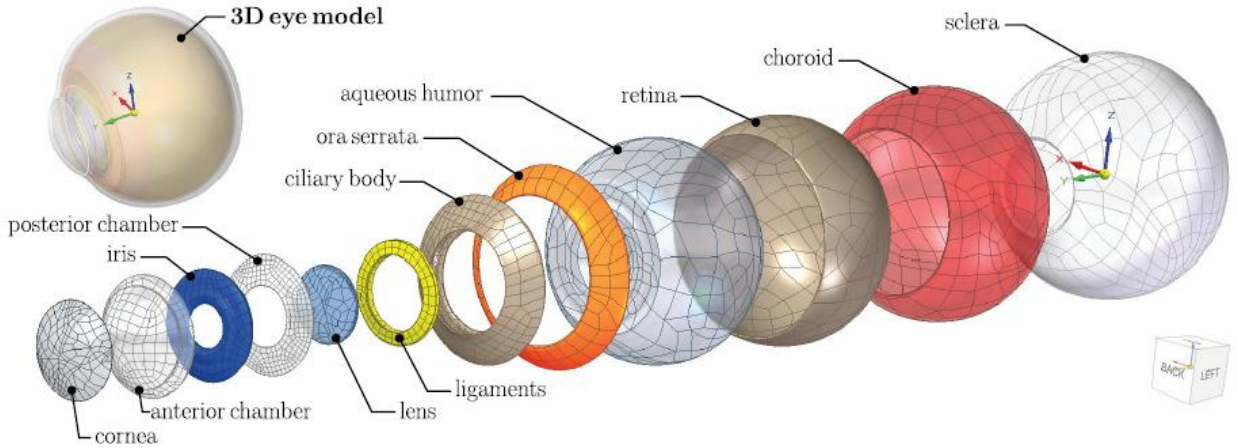

EM fields computation

- To reduce the computational cost it makes sense to reduce the number of unknowns at computational boundary Γ
- This is achieved by submerging the head into airbox

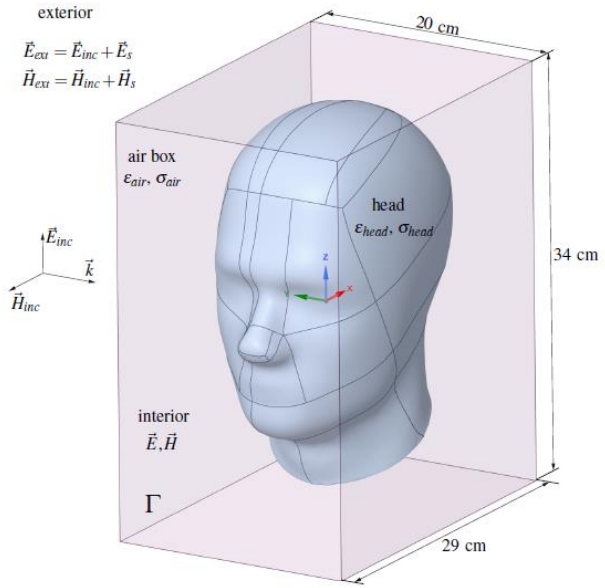

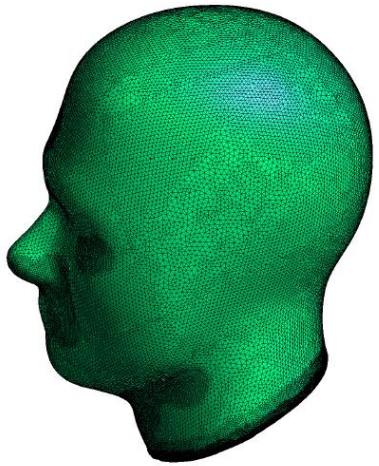

Fig. 3. The surface of the phantom head is represented by 151,185 triangles, and the interior of the head is represented by 3,511,924 tetrahedrons.

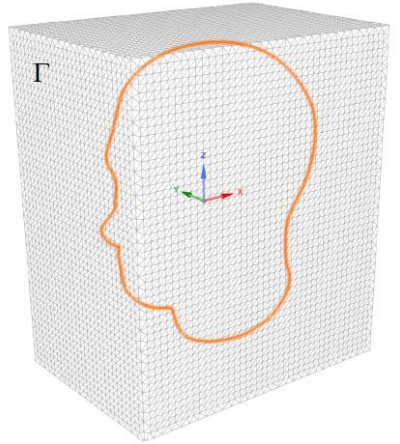

Fig. 4. The surface of the airbox is discretized using only 8,984 triangles yielding 13,476 unique edges, and $2 \times 13,476$ unknown coefficients e_b and h_b at the surface Γ.

EM fields computation

- Without air-box the surface of the human head is highly irregular – 151,185 triangles to model detailed human head geometry
- The required storage for BEM submatrices is roughly 2 TB (terrabytes)
- Direct solvers (e.g. Intel Pardiso) would require many more terabytes of RAM
- The size of system matrix can be greatly reduced if we place the head in airbox – regular surface – but now the model is inhomogeneous
- Airbox is modeled with only 8,984 triangles (respecting $\lambda/10$ criteria)
- Storage requirement for BEM part 2.7 GB
- Surface of the human head is still complex - 151,185 triangles

EM fields computation

- The results of EM field computation for frequency f=2.45 GHz (homogenous IEEE SAM model)

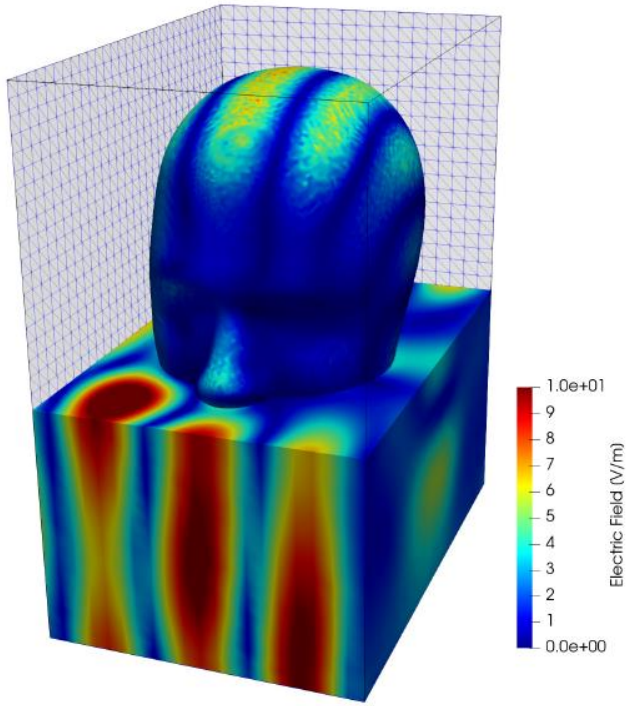

Fig. 6. The magnitude of the induced electric field on the surface of human head phantom and in the surrounding air. The airbox was cut at the nose, and only the lower portion of the airbox is shown.

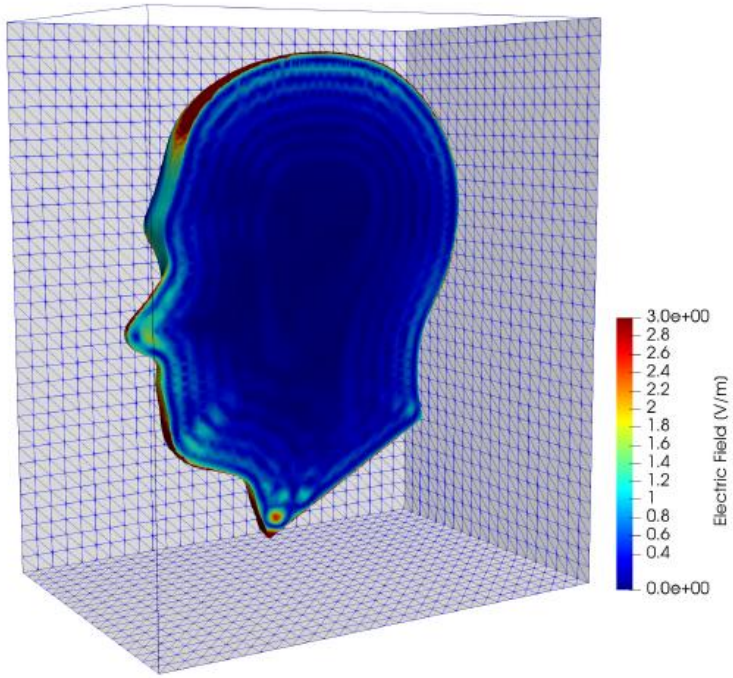

Fig. 7. The magnitude of the induced electric field inside human head phantom. The airbox is not shown. The wavelength of EM waves has shortened because ϵ_r in head is larger than in air.

Excitation: plane wave with power density $100\ mW/m^2$

Element size: no element is larger than $\lambda/10$

Model size: 7,926,464 tetrahedral elements, 3,511,924 for head and 4,414,540 for air

Thermal rise computation

- Once the EM field distribution in the human head is computed, we proceed to thermal rise computation
- To compute thermal rise we solve Pennes' bio-heat equation

$$\nabla \cdot (\lambda \nabla T) + W_b c_b (T_a - T) + \dot{Q}_m + \dot{Q}_{em} = 0$$

- Electromagnetic heat sources come from SAR:

$$\dot{Q}_{em} = \rho SAR$$

- And SAR is computed from the electric field:

$$SAR = \frac{\sigma}{2\rho} \left| \vec{E} \right|^2$$

Thermal rise computation

- For thermal rise computation the method of choice is FEM – simplest, nodal elements
- At the bounding surface of the head the Neumann boundary condition is imposed

$$\lambda \frac{\partial T}{\partial \vec{n}} = \lambda \left(\vec{n} \cdot \nabla T \right) = -h_c \left(T - T_{amb} \right)$$

- Ambient temperature $T_{amb} = 22°\mathrm{C}$
- $h_c = 20 W/m^2 °\mathrm{C}$

TABLE I
ELECTRICAL AND THERMAL PROPERTIES

Property	Symbol	Units	Head	Air-box
Conductivity	σ	$\frac{\mathrm{S}}{\mathrm{m}}$	1.8	0.0
Relative permittivity	ϵ_r		39.1	1.0
Mass density	ρ	$\frac{\mathrm{kg}}{\mathrm{m}^3}$	1000.0	1.225
Thermal conductivity	λ	$\frac{\mathrm{W}}{\mathrm{mK}}$	0.41	0.03
Blood perfusion	W_b	$\frac{\mathrm{W}}{\mathrm{m}^3\mathrm{K}}$	7443.786	0.0
Metabolic rate	$\dot{Q}_m$	$\frac{\mathrm{W}}{\mathrm{m}^3}$	0.0	0.0

Thermal rise computation

- FEM formulation is based on the weighted residual method of Galerkin:

$$\int_V N_i \left[\nabla \cdot (\lambda \nabla T) + W_b c_b (T_a - T) + \dot{Q}_m + \dot{Q}_{em}\right] dV = 0$$

- Weak formulation:

$$\int_V [\lambda \nabla N_i \cdot \nabla T + N_i W_b c_b T]\, dV + \oint_\Gamma h_c N_i T dS = \quad (15)$$
$$\int_V N_i \left[W_b c_b T_a + \dot{Q}_m + \rho SAR\right] dV + \oint_\Gamma h_c T_{amb} N_i dS$$

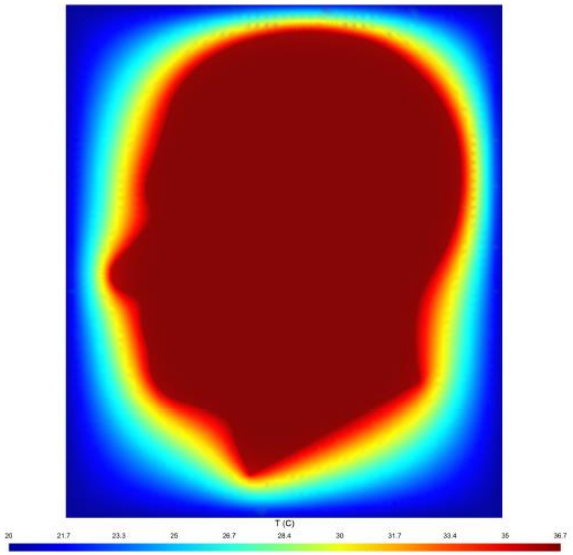

Fig. 8. The cross section of the temperature field in the $x - z$ plane.

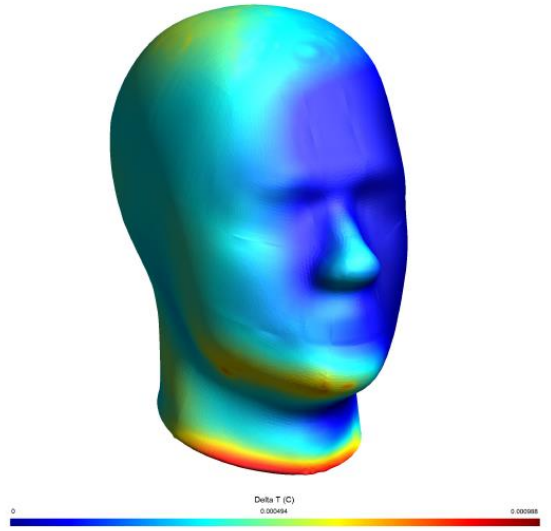

Fig. 9. The temperature increase on the surface of the human head phantom caused by the time harmonic EM fields with power density of $100\,\mathrm{mW/m^2}$.

Some Results

- Wavelength shortens inside human head (for air $\lambda = 12.23\ cm$, inside head $\epsilon_r = 39.1$, $\lambda = \frac{c}{f} = \frac{1}{\sqrt{\mu\varepsilon}f} = 1.95cm$)
- For bluetooth frequencies f=2.45 GHz dominant heating effect is at the surface of the human head
- This is due to small penetration depth $\delta = \frac{1}{\sqrt{\pi f \mu\sigma}} \approx 7mm$
- At $100\ mW/m^2$, f=2.45 GHz,heating effects were not significant

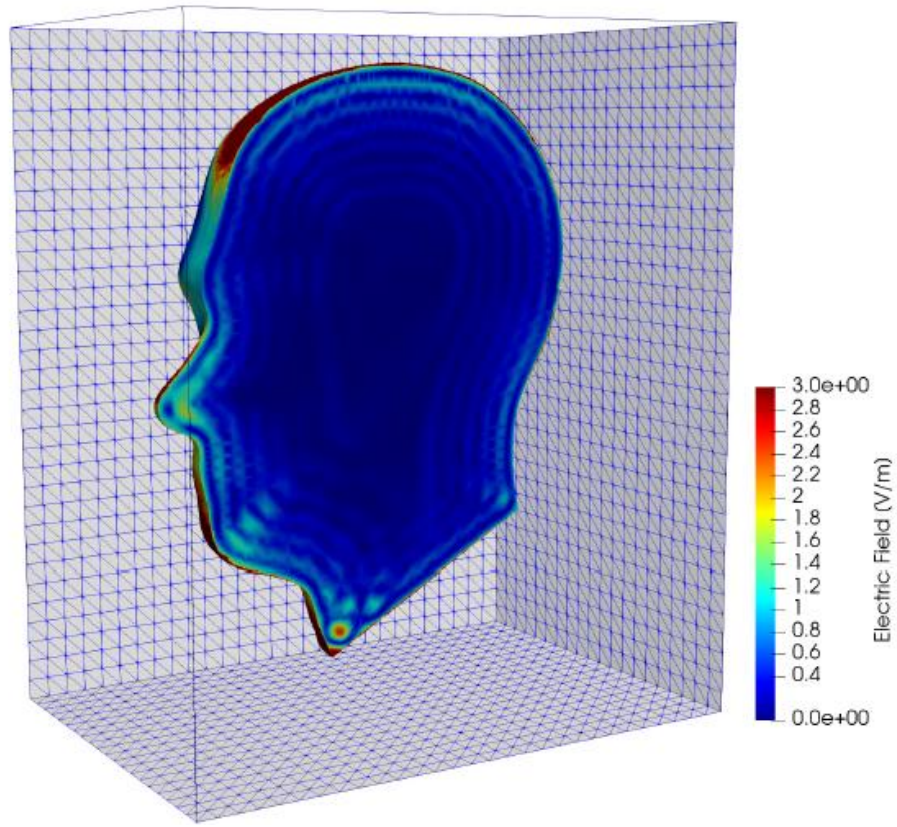

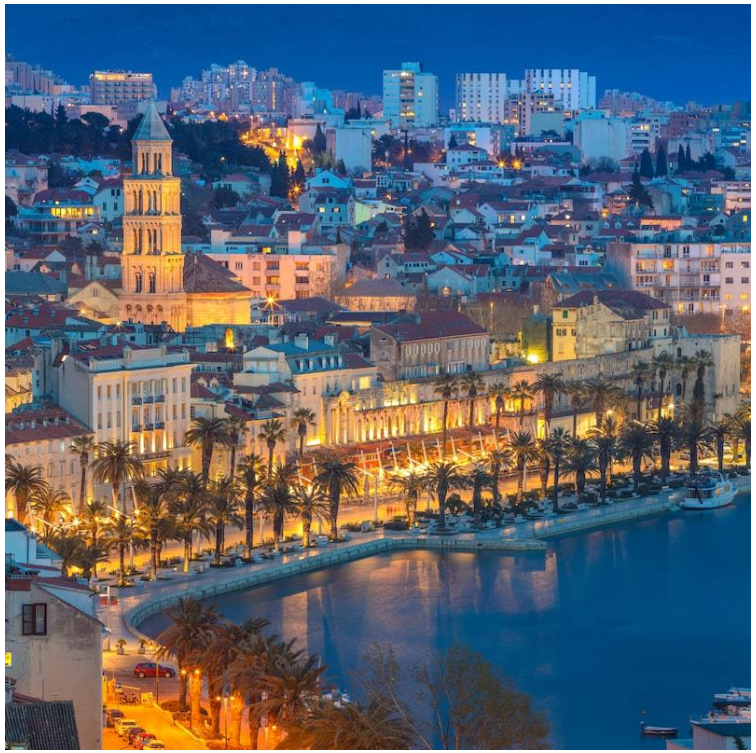

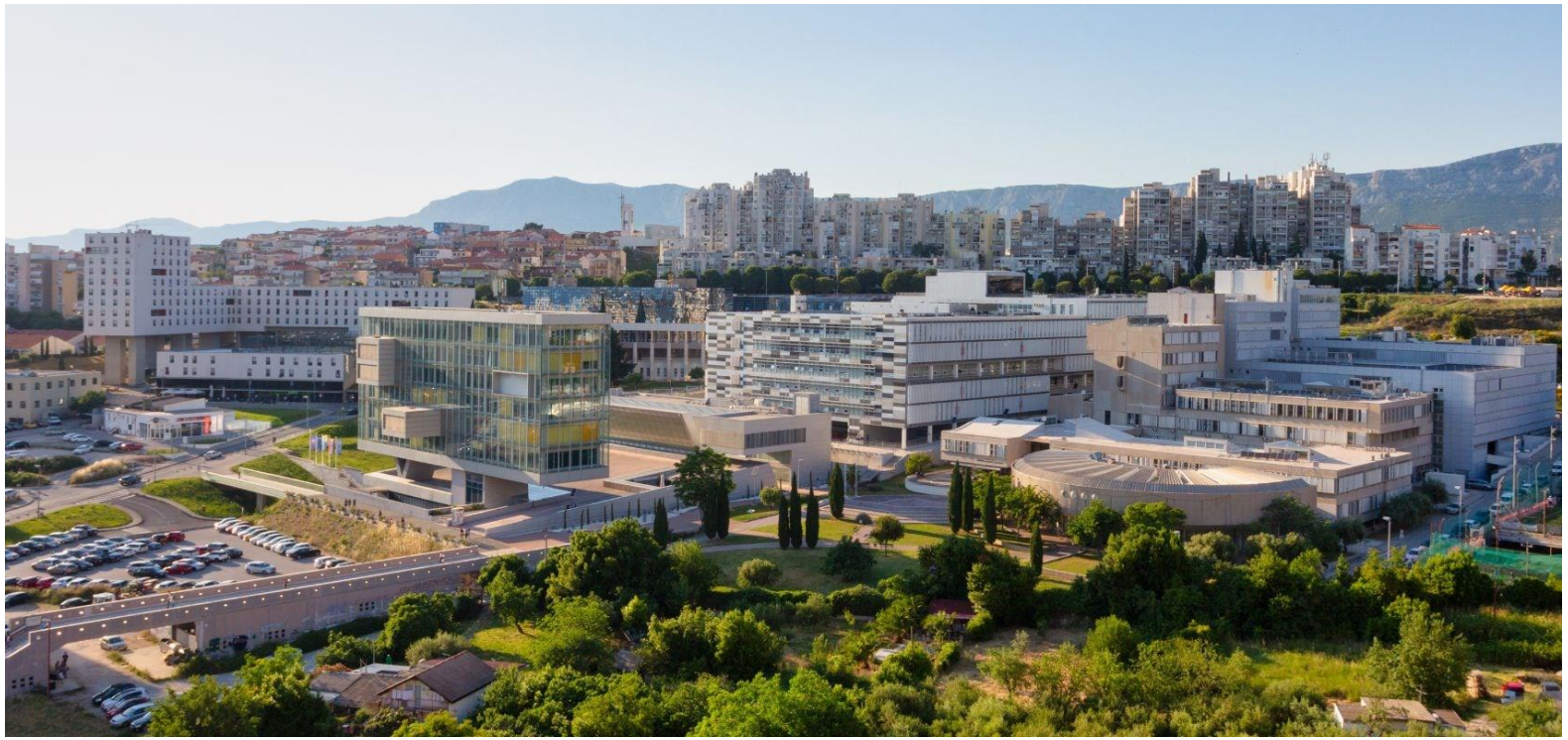

Thank you for attention!

H. Dodig, K. Viđak, M. Škiljo, D. Poljak
University of Split, Croatia